Journal of Materials Chemistry C

ROYAL SOCIETY OF CHEMISTRY

PAPER

View Article Online
View Journal | View Issue

Cite this: J. Mater. Chem. C, 2021, 9, 4544

Electromechanical coupling of isotropic fibrous networks with tailored auxetic behavior induced by water-printing under tension†

Jinyuan Zhang,[a] Sheila M. Goodman,[b] Heather G. Wise,[b] Anthony B. Dichiara [b] and Jae-Hyun Chung *[a]

Received 25th November 2020,
Accepted 12th March 2021

DOI: 10.1039/d0tc05526c

rsc.li/materials-c

Understanding the electromechanical coupling of auxetic materials offers unique opportunities to enhance the sensitivity of piezoresistive sensors. Reports on the auxetic behavior of random fiber networks have been relatively scarce due to their less pronounced Poisson's expansions than other auxetic designs adapting periodically arranged structures. In this study, the auxetic response of hierarchical pulp-carbon nanotube networks is tailored through the localized tensional micro-fracture initiated by water-printing. The interfacial junctions among multiwalled carbon nanotubes (MWCNTs) and cellulose fibers are disintegrated and reorganized to induce the buckling of a wet CNT paper composite (CPC) network. The Poisson's ratio of −49.5 is achieved at the water-printed region. The resulting piezoresistive properties of CPC sensors exhibit high sensitivity (3.3 kPa^{-1}) over a wide dynamic range (6–500 000 Pa). The novel auxetic behavior of water-printed CPC paves the way for high performance and inexpensive wearable devices.

Introduction

Auxetic materials, characterized by their negative Poisson's ratios, expand in the transverse direction under uniaxial stretching.[1] This distinctive trait offers unique mechanical properties, namely indentation resistance, fracture toughness, and shear resistance, which makes auxetic materials appealing in diverse fields, such as tissue engineering,[2] aerospace,[3] and sports.[4] While the elastic theory constrains the Poisson's ratio to a range between −1 and 0.5,[5] a computational study reported an in-plane Poisson's ratio of −17 for an auxetic structure comprising rotachiral lattices.[6] Additional research provided further guidelines to design auxetic structures with large Poisson's ratio based on a programmed geometric layout for highly deterministic and periodic structures.[7,8]

However, the manufacturing of periodically arranged structures for practical applications remains challenging, while random structures are typically associated with modest Poisson's ratios. Recent experimental and computational results found that certain individual fibers oriented transversely in a random network can experience microscale buckling, yielding extreme Poisson's ratios up to −400.[9] This phenomenon was only observed locally at the scale of individual fibers. The present research aims at controlling the buckling effect in a random fibrous network to produce auxetic materials with large Poisson's ratios in a simple and economic fashion for multifunctional sensing applications.

Auxetic-based resistive sensors have been developed for various applications ranging from healthcare,[10–13] to human-machine interfaces,[14–16] and automations.[17,18] According to the percolation theory, the rapid increase of resistance occurs when the strain becomes greater than a critical value. Beyond this threshold value, the percolated conductive network is drastically terminated to reduce the number of electrical paths in the material.[20,22,23] In conventional materials, the disruption of the percolated conductive network is compensated by the reorganization of electrical paths in the out-of-plane direction due to Poisson's contractions. The piezoresistive sensitivity of auxetic materials can be amplified by the out-of-plane expansions in the auxetic structure.[25–29] Furthermore, in response to a compressive load exerted on the surface, auxetic sensors exhibit a larger dynamic range in comparison to analogous conventional materials. Their superior sensitivity to strain makes the sensors particularly suited for delicate vibration monitoring, such as wrist pulse.[22,23] Compared to traditional strain and pressure gauges, novel electromechanical coupling mechanisms have been proposed,[19] such as disconnection of sensing

[a] Department of Mechanical Engineering, University of Washington, Seattle, WA 98195, USA. E-mail: jae71@uw.edu
[b] School of Environmental and Forest Sciences, University of Washington, Seattle, WA 98195, USA

† Electronic supplementary information (ESI) available. See DOI: 10.1039/d0tc05526c

elements,[20,21] tunneling effect,[22,23,30] and fracture-induced sensitivity,[24] which offers new routes to optimize the sensitivity of piezoresistive materials. This manuscript represents, to the best of our knowledge, the first report studying the electromechanical coupling of random networks with auxetic properties.

Paper made of cellulose, the most abundant natural polymer extracted from woody biomass, benefits low-cost, lightweight, and large surface area. The nonwoven structure of cellulose fibers provided the random networks with auxeticity.[31,32] This auxetic material showed piezoresistivity when assembled with sensing elements.[33–36] However, the low auxeticity of cellulose fiber networks barely contributed to the sensitivity. The constraints of inter-fiber junctions hampered large deformations of cellulose network and disconnections of molecular junctions. Our previous work showed that the fracture of cellulose paper composites (CPC) reorganized the cellulose networks, which provided an insight for the in-plane electromechanical coupling of the random networks under structural reorganization.[24] However, the inconsistent and dispersive fracture showed unpredictable sensitivity, and the contribution of the auxetic behavior was not clear.

This paper presents a novel way to control the fracture of CPC with a great spatial resolution based on a simple and scalable water-printing method to enhance the auxetic behavior of fibrous composites for highly sensitive piezoresistivity. Pristine and fractured CPC's microstructures are characterized by optical and electron microscopies. A noncontact printing of water can locally weaken the hydrogen bonds and soften the pulp fibers for controlled fractures. The auxetic mechanism induced by the wetting process is investigated in conjunction with the piezoresistive sensitivity. The produced CPC piezoresistive sensors are characterized for sensitivity, dynamic range, and reproducibility and are applied to multiple wearable devices, such as pulse detection, breath monitoring and walk pattern recognition. The acquired auxetic behavior from the random network structures opens the way to develop high-performance and low-cost sensors for a large variety of applications in portable electronics.

Experimental

Materials

Bleached Kraft softwood pulp (SW) was kindly provided in a dried mat form from Port Townsend paper mill. Alkali lignin (AL, 99%), sodium dodecyl sulfate (SDS, 99%), and cationic polyacrylamide (CPAM, Percol 3035) were obtained from Tokyo Chemical Industry Co., MP Biomedicals, and BASF, respectively. Hydroxyl-functionalized carbon nanotubes (CNT-OH), synthesized from catalytic chemical vapor deposition, were purchased from Cheap Tubes Inc. As per the manufacturer data, CNT-OH have lengths in the 10–20 μm range and mean diameter of 50 nm, with an average of 5.5% of OH groups. All chemicals were used as received without any additional treatment.

CPC preparation

CNT-cellulose composite papers were prepared following a modified TAPPI T-205 standard method, as previously reported elsewhere.[37] Briefly, handsheets were formed by a filtration method using a handsheet molder (Essex International Inc. Custom Machinery), and pressed and dried according to TAPPI T-205 standards. Prior to sheet formation, CNT-OH were dispersed in a binary mixture of AL and SDS (90 : 10 wt) using a double acoustic irradiation system, to promote individualization in solution and achieve a uniform distribution of charge transport routes throughout the final composite.[38] Aqueous dispersion of CPAM were first added to pulp fiber solutions (0.3% consistency) and combined on a hot plate at 50 °C for 30 minutes. The as-dispersed CNT-OH solutions were then added to the pulp mixture, and kept under constant agitation for 30 minutes. The combined CNT-OH and pulp suspensions were then filtered, pressed, and dried to form handsheets. The proportion of cellulose fibers, CNTs, CPAM, AL, and SDS were adjusted to achieve a total mass of 1.2 g OD (60 g m^{-2}). For comparison purposes, handsheets were also prepared without any CNT-OH, just using a pulp/CPAM/AL/SDS blend and denoted as "control" samples. All handsheets were kept for 48 hours under room temperature conditions (23 °C) and 50% relative humidity prior to testing. All handsheets had a mean thickness of 88.4 ± 3.1 μm.

Fabrication of the CPC piezoresistive sensors by water-printing

CPC piezoresistive sensors were fabricated by controlled water-printing and stretching. Silver paste (MG Chemicals, USA) was applied to both ends of the CPC strip and cured at 70 °C on a hot plate to make the electrodes. The water was printed on CPC specimens by using a noncontact printing method. Using a liquid bridge printing method, constant water volume was supplied each run by maintaining a consistent contact angle and printing speed.[39] Using a 0.8 mm-diameter capillary pen, water was printed repeatedly with a 3-dimensional controller. The stretching was applied by a tensile test stage in a humidity chamber (Fig. 1). A boiled water source was supplied in the chamber to maintain a humidity of 80% at 28 °C. Under this

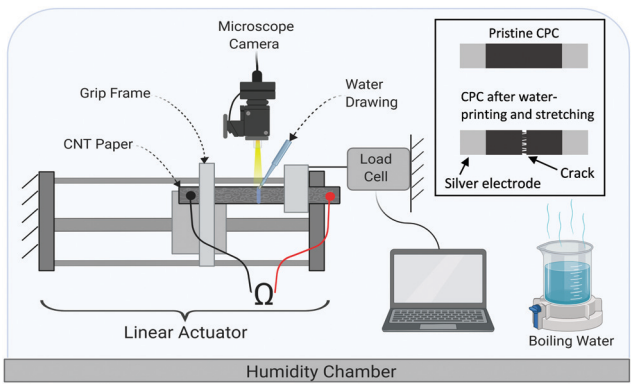

Fig. 1 Schematic describing the production of auxetic CPC by water-printing under uniaxial tension. The inset shows the CPC before and after the water-printing and stretching process.

controlled environment, the printed water volume on the CPC was kept constant during the test by preventing evaporation. Regarding the stretching test, the strain was defined by $\varepsilon = \frac{L - L_0}{L_0}$, where L is the length of the specimen under stretching, and L_0 is the original length (10 mm) of the specimen. The fracture strain was defined to be the strain at the fracture under stretching. For reproducible fabrication procedures, force and resistance were recorded by a load cell (DYMH-103, CALT, China) and a multimeter (Fluke Corp., USA), respectively. The stress was calculated by $\sigma = \frac{F}{D \times T}$, where F was the force measured by the load cell, D was the pristine width of the specimen, and T was the thickness of the specimen measured by a digital gage (PK-0505, Mitutoyo, Japan).

Auxetic behavior characterization

The auxetic behavior of the CPC was studied by measuring the thickness changes. In the setup of the CPC sensor fabrication stage (Fig. 1), a stereo zoom microscope was focused on the water-printed region of the specimen from the transverse direction of the stretching. The thickness change of the specimen during the water-printing and stretching was measured using optical microscope images and ImageJ software. The measured thickness was also validated by a scanning electron microscopy (SEM, XL830, FEI Company, Hillsboro, OR, USA) study. The thickness was compared for pure paper, and CPC with the CNT concentrations of 2.5, 5, and 10 wt%. The instantaneous Poisson's ratio (ν_{inst}) and effective Poisson's ratio (ν_{eff}) were computed based on the following equations:[40]

$$\nu_{inst} = -\frac{(z_i - z_{i-1})/z_{i-1}}{(l_i - l_{i-1})/l_{i-1}} \quad (1)$$

$$\nu_{eff} = -\frac{(z_i - z_0)/z_0}{((l_i - l_0))/l_0} \quad (2)$$

where l_i and z_i denoted the specimen length and thickness values at the given strain level, and l_{i-1} and z_{i-1} denoted their values at the previous level. l_0 and z_0 denoted the original specimen length and thickness. l_0 was 10 mm, containing the wet, semi-wet and dry regions after water-printing. For the specimens with the water-printed CPC six-times, CNT contents were 0, 2.5, 5, and 10 wt%. ν_{inst} was computed at the strains of 0.02, 0.03, 0.04, 0.05, 0.08 and 0.10. ν_{eff} of six-time water-printed paper and CPCs were computed at strain of 0.01, 0.02, 0.03, 0.04, 0.05, 0.08 and 0.10. The ν_{eff} of non-water-printed paper and CPCs were computed at their fracture strain. The ν_{eff} of non-water-printed specimens at fracture strain was compared with that of six-time water-printed specimens that had maximum magnitudes.

Characterization of the anisotropy of fractured CPC

SEM (XL830, FEI Company, Hillsboro, OR, USA) was used to study the CPC surface morphology in-plane and fracture length. The CPC 2.5 wt% was sputter-coated with gold/palladium with the thickness of 6–7 nm. To ascertain the fracture length and morphology, the CPC was mounted to a flat aluminum stage using carbon tape and imaged using a 5 kV accelerating voltage with a 5 mm working distance. Fracture length and pulp fiber orientation were determined using Image J software and the following equation:

$$f_c = \frac{\mathrm{FWHM} - 180}{180} \quad (3)$$

FWHM represented the full width half maximum of the peak created from the Gaussian fit conducted on the alignment histogram. UV-vis measurements were performed on a PerkinElmer Lambda 750 spectrophotometer equipped with a 100 mm-integrating sphere operating in the 450–850 nm range. CPC samples were mounted on top of a 3 mm-diaphragm, and a polarizer was used to capture anisotropy. For the convenience of the discussions of orientations, the stretching direction was defined to be x-direction, the in-plane direction perpendicular to x-direction was y-direction, and the out-of-plane direction was z-direction. Determined by their angles to x-direction, cellulose fibers in x–z plane were categorized into tilted and inclined fibers.

Characterization of piezoresistive sensitivity

Piezoresistive force sensors were fabricated by the water-printing and stretching method. CPC with 0, 2.5, 5, and 10 wt% CNT were used with the six times of water-printing and 0.1-strain. A straight water line was printed on the CPC samples. The piezoresistive sensitivity was characterized by a PDMS block integrated with a load cell (Fig. 1). The dimension of the PDMS block was $7 \times 15 \times 2$ mm^3 to completely cover the fracture area (approximately 1.5×5 mm^2). The linear actuator was controlled to apply the repeated force between 0 and 500 kPa at a speed of 55 μm s^{-1}. A multimeter was connected to the sensor to measure the resistance change when the sensor was pressed. The sensitivity of the sensor was $S = (\Delta R/R_0)/\Delta p$, where ΔR was the resistance change of the sensor, R_0 was the initial resistance of the sensor, and Δp was the change of the applied pressure. The error bars were calculated to study the reproducibility of the sensor's sensitivity. The dynamic range (DR) was defined as $\mathrm{DR} = \frac{P_{high}}{P_{low}}$, were P_{high} and P_{low} were the highest and lowest pressure that could be measured by a sensor.

To demonstrate sensor applications, heartbeat, respiration, and gait movement were measured. The sensors were tested by de-identified volunteers. Among the testing results from multiple volunteers, a randomly chosen secondary data set was demonstrated for sensing performance evaluation.

Results and discussion

Tailored auxetic behavior of CPC for sensor fabrication

The water-printing method provided scalable fracture-induced fabrication of piezoresistive sensors based on a random network of cellulose fibers pre-adsorbed with CNTs (Fig. 1). Pristine CPCs consist of randomly oriented pulp fibers embedded

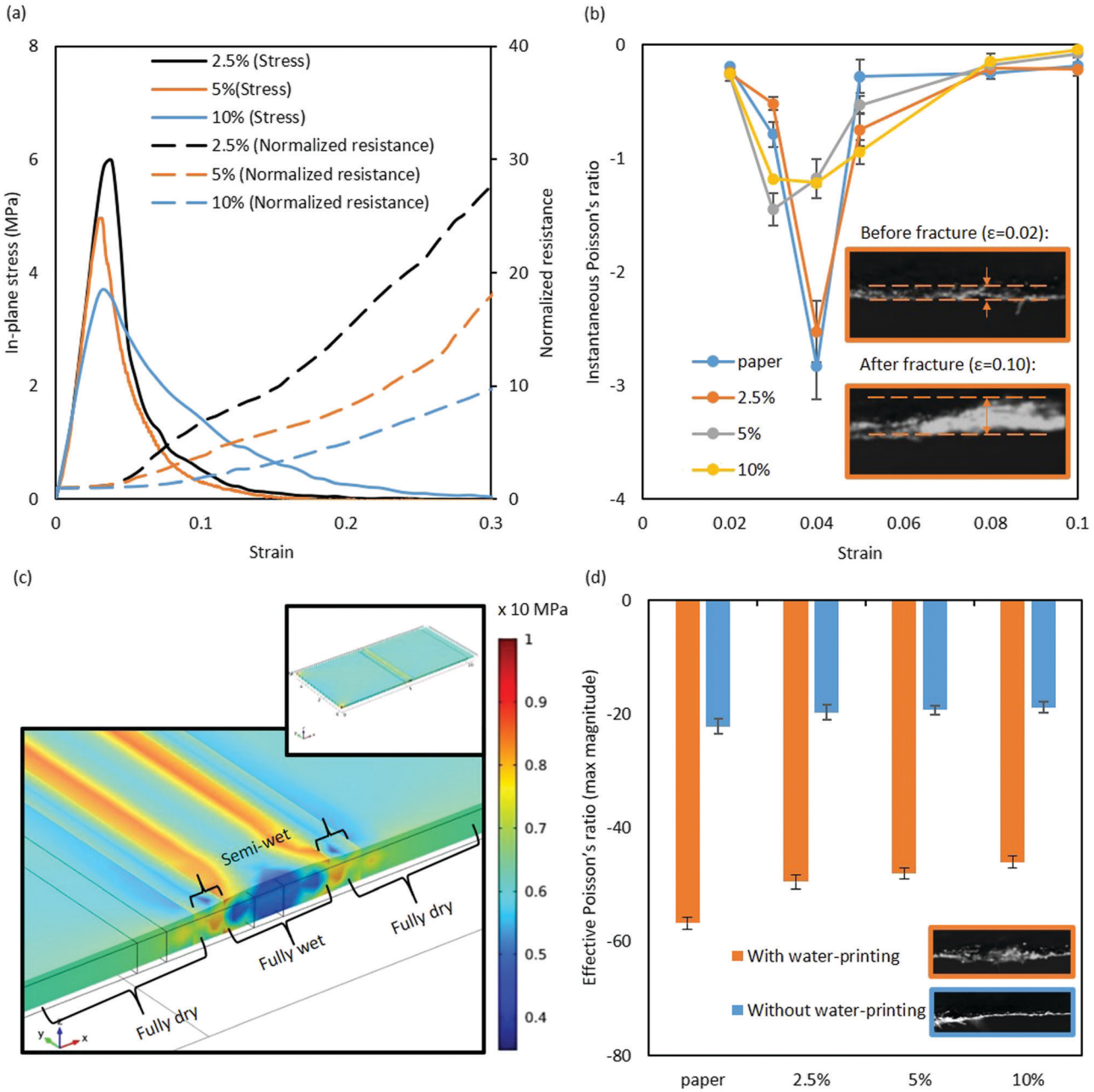

Fig. 2 (a) Stress–strain relationship coupled with normalized resistance change. (b) Instantaneous Poisson's ratios of pure paper and CPC with CNT wt% of 2.5, 5 and 10 during stretching. Inset: Optical images of CPC profiles with 2.5 CNT wt% before and after fracture (ε = 0.02 and 0.10). The original CPC thickness is 100 μm. (c) Simulation result of stress distribution for water-printed CPC under tension. (d) Maximum effective Poisson's ratios for water-printed and non-water-printed pure paper and CPC with CNT wt% of 2.5, 5, and 10. Inset: Optical microscope images of fractured profiles of CPC with 10 CNT wt% with and without water-printing.

with well-dispersed CNTs with no obvious aggregations (Fig. S1, ESI†). The water-printing applied by a capillary pen enabled the non-contact wetting with a desired pattern. Water ink was supplied through an ink bridge formed between the pen nib and the substrate. The water-printing flow rate was kept constant among all samples through control of the pen tip height from the substrate, contact angles, and printing speed.[39] Using the liquid-bridge printing method, accurate water lines could be printed repeatedly without damaging the substrates. After the water-printing was repeated six times, the sample was stretched until fracture and its electrical resistance was recorded. The strain was applied until 0.3 where the stress magnitude for all stretched specimens became 0. The electro-mechanical coupling of CPC prepared at various CNT loadings (*i.e.* 2.5, 5, and 10 wt%) was studied during uniaxial stretching, as shown in Fig. 2a. It can be observed that the onset of resistance changes due to in-plane stretching corresponds to the largest variations in the instantaneous Poisson's ratios (Fig. 2b).

This electromechanical coupling offers a simple method to streamline the manufacturing of auxetic CPC by measuring the electrical resistance. The mechanical properties of the composites that are water-printed for 0, 2, 6, and 10 times are presented for the CPC with all three CNT contents (Fig. S2a–c, ESI†). As the indications of reproducibility of mechanical properties of water-printed CPC, the fracture strain, ultimate strength, and wet strength retention of CPC of 2.5, 5, and 10 wt% are demonstrated with the water-printing times of 0, 2, 4, 6, 8 and 10 (Fig. S2d and e, ESI†). The fracture strain and ultimate strength were reduced by the increased number of water-printing, and meanwhile the reproducibility increased. For the CPC of 2.5 wt%, the fracture strain and ultimate strength were 0.026 ± 0.0031 and 6.6 ± 0.11 MPa with six times of water-printing, and 0.046 ± 0.0037 and 25 ± 1.3 MPa without water-printing. The reduced deviations of the ultimate strength were obtained by the localized, predictable wet fracture process of CPC.

To eliminate the effect of strength difference among non-water-printed CPC with different CNT contents, the strength reduction by water-printing on CPC was reflected by their wet strength retention. The wet strength retention was defined as the ratio of the average ultimate strength of water-printed CPCs to that without water-printing (Fig. S2f, ESI†). A two-time water-printing significantly reduced the wet strength retention to 35–45%. The strength reduction began to saturate at six-time water-printing, when the wet strength retention reached 19–26%. Therefore, the six-time water-printing was selected for fracture manipulation. The CPC with higher CNT wt% showed the lower wet strength retention, indicating that the water-printing method had the greater reduction of CPC strength with the lower CNT content. This was attributed to the greater hydrophilicity with more hydroxyl-functionalized CNTs embedded on cellulose fibers, which was supported by the contact angles (Fig. S3, ESI†). The different wetting characteristics were demonstrated by contact angle measurements averaged over six replicates. The 2.5 wt%-CPC and 10 wt%-CPC yielded the contact angles of 91.5 ± 0.7° and 88.5 ± 0.5°, respectively, resulting in a greater diffused wet area at higher CNT contents (Fig. S4, ESI†). This observation was consistent with the fractured length determined at various CNT content and under the same applied strain (Fig. S5, ESI†).

The electromechanical properties of CPC were depicted as a two-stage resistance response, including the slow increase of resistance before an inflection point followed by the rapid increase. The inflection point was declared when the stress–strain curve deviated from the linear slope by 5%. The two stage increase of the resistance was dominated by the breakage of CNTs spanning the cellulose fibers (Fig. S6, ESI†), and the fracture-induced rapid reduction of tunneling effects, respectively.[41] The slow and rapid resistance increases at low and high strains were qualitatively consistent with the piezoresistive properties of other CNT composites.[24,42] The normalized resistances at 0.3-strain were 27.3, 18.7, and 10.1 for the CPC with 2.5, 5, and 10 CNT wt%, respectively. The higher normalized resistance of CPC with lower CNT content after fracture indicated less retained electrical paths.

It was discovered that the water-printing amplified and localized the out-of-plane directional auxeticity of CPC by predictable fractures. The thickness view of the optical microscope images showed that the auxetic behavior of random CPC networks was locally induced by the controlled fracture developed *via* the water-printing method (Fig. S7, ESI†). The instantaneous Poisson's ratio (ν_{inst}) was measured to assess the auxetic behavior of CPC at representative strain values (Fig. 2b), which indicated the instantaneous increase of the specimens' thickness at certain strains. The Poisson's ratio ranged −0.26 to −0.19 in the elastic range (strain < 0.02), where the fibers were forced to expand the thickness in the transverse direction due to the stretching. The drastic augmentation in thickness occurred at the plastic deformation range of 0.03–0.04 strain, indicated by the highest magnitude of ν_{inst}, which was synchronized with CPC's stress increase in Fig. 2a. The ν_{inst} remained negative until strain of 0.10, indicating the continuous increase of the thickness. When the applied strain was greater than 0.10, ν_{inst} became 0. Due to the instant, unpredictable fracture process, ν_{inst} for non-water-printed specimens was not measured. The localized and predictable fractures by water-printing opened a way to study the mechanical properties and plastic deformation of random network structures.

The localized fracture of water-printed CPC was attributed to the reduced strength of cellulose fibers and the stress concentration induced by water-printing (Fig. 2c). Finite element analysis (FEA) demonstrated that the stress was concentrated at the semi-wet region between the fully wet and dry regions of CPC due to the localized auxetic behavior and the different stiffness of wet and dry CPC (Fig. S8, ESI†). To assess the contribution of auxetic behavior and stiffness difference to the stress concentration, the stress concentration factor (K_t) was defined as the ratio of the maximum stress (σ_{max}) to the stress without auxetic behavior and stiffness difference (σ_0). When only the auxetic behavior was considered in the numerical analysis, K_t was 1.3 (Fig. S8e and h, ESI†). Considering only the stiffness difference, K_t was 1.4 (Fig. S8f and i, ESI†). Due to the numerical errors resulting from the large magnitude of negative Poisson's ratio, the simulation was conducted in the small strain range below 0.02. The applied strain and the magnitude of Poisson's ratios in wet and semi-wet regions were much smaller than those under fracture. Apparently, K_t will increase as the difference of Poisson's ratios enlarge. In combination with the stress concentration at the semi-wet region, the fracture was initiated at the center of the wetted region due to the significant strength reduction of the wet CPC. The necking showing the reduced width occurred at both the semi-wet and fully wet regions.

The remarkable auxeticity was induced by fracture and enhanced by the water-printing. The auxeticity of a specimen was indicated by ν_{eff}, which showed the averaged Poisson's ratio from 0 to a certain strain level. The maximum ν_{eff} magnitudes (ν_{effmax}) of water-printed specimens were obtained slightly after fracture (strain = 0.04–0.05) (Fig. S9, ESI†). Since the ν_{effmax} indicated the greatest auxeticity of a CPC specimen

under stretching, the magnitude of ν_{effmax} was chosen for the quantitative comparison of auxeticity of paper and CPC specimens. The maximum thickness and ν_{effmax} of non-water-printed specimens were obtained at the fracture (strain = 0.02–0.03) as illustrated by the cross-sectional micrographs in Fig. S10 (ESI†). The effect of the water-printing process on the auxetic behavior of the fibrous composites was assessed by comparing the ν_{effmax} of water-printed and non-water-printed specimens (Fig. 2d). The ν_{effmax} values of water-printed paper and CPC with 2.5, 5, and 10 CNT wt% were significantly greater than their fully dry counterparts by 2.6, 2.5, 2.5 and 2.3 times. It was also found that the ν_{effmax} values of the fully wet CPC were 1.9, 1.9, 1.8 and 1.7 times those of the non-water-printed counterparts. Regardless of water-printing, the lower CNT contents consistently yielded the more pronounced auxetic behavior. For instance, the ν_{effmax} of water-printed 2.5%-CPC was −49.5, which was 1.09 times that of 10%-CPC. Remarkably, the ν_{effmax} of water-printed paper raised to −56.7 in the absence of CNTs.

Mechanisms of fracture-induced auxetic behavior of CPC

To understand the underlying mechanism of fracture-induced auxetic behavior tailored by water-printing, SEM study was conducted at various representative stages of stretching to investigate in-plane and out-of-plane orientations of fibers (Fig. 3a–d). The fiber orientation within stretched CPC of 2.5 wt% was plotted at 0, 0.03, and 0.10 strain (Fig. 3a–c). The orientation factor, f_c, ranging from 0 (fully isotropic) to 1 (perfect alignment) was determined. Localized at the fractured region of the specimens, the fiber alignment to the stretching direction increased under applied strain, regardless of CNT contents. The observation was consistent with polarized absorption spectroscopy data confirming the optical anisotropy was observed only at the fractured region of the strained samples (Fig. S11, ESI†). The fiber orientations of CPC at 5 and 10 wt% loading are presented in Fig. S12 (ESI†). The CPC with the lowest amount of CNT (*i.e.* 2.5 wt%) exhibited the highest degree of fiber orientation, with a f_c of 0.77 at a strain of 0.10, and the largest auxeticity with a Poisson's ratio of −31.0 (Fig. S9, ESI†). The significant fiber reorientations in z direction were verified by SEM images (Fig. 3d). Different from the compact layers within a pristine cellulose fiber matrix, the fractured CPC showed larger inter-fiber distances. After the fracture, broken cellulose fibers at fractured region lifted towards z direction and formed larger angles to the x–y plane, exhibiting much larger thickness at fractured region. The optical images showing the in-plane and out-of-plane geometries at the fractured regions on the CPC were shown in Fig. 3e. From the in-plane view, necking was observed at the water-printed region on CPC, where the thickness was also the

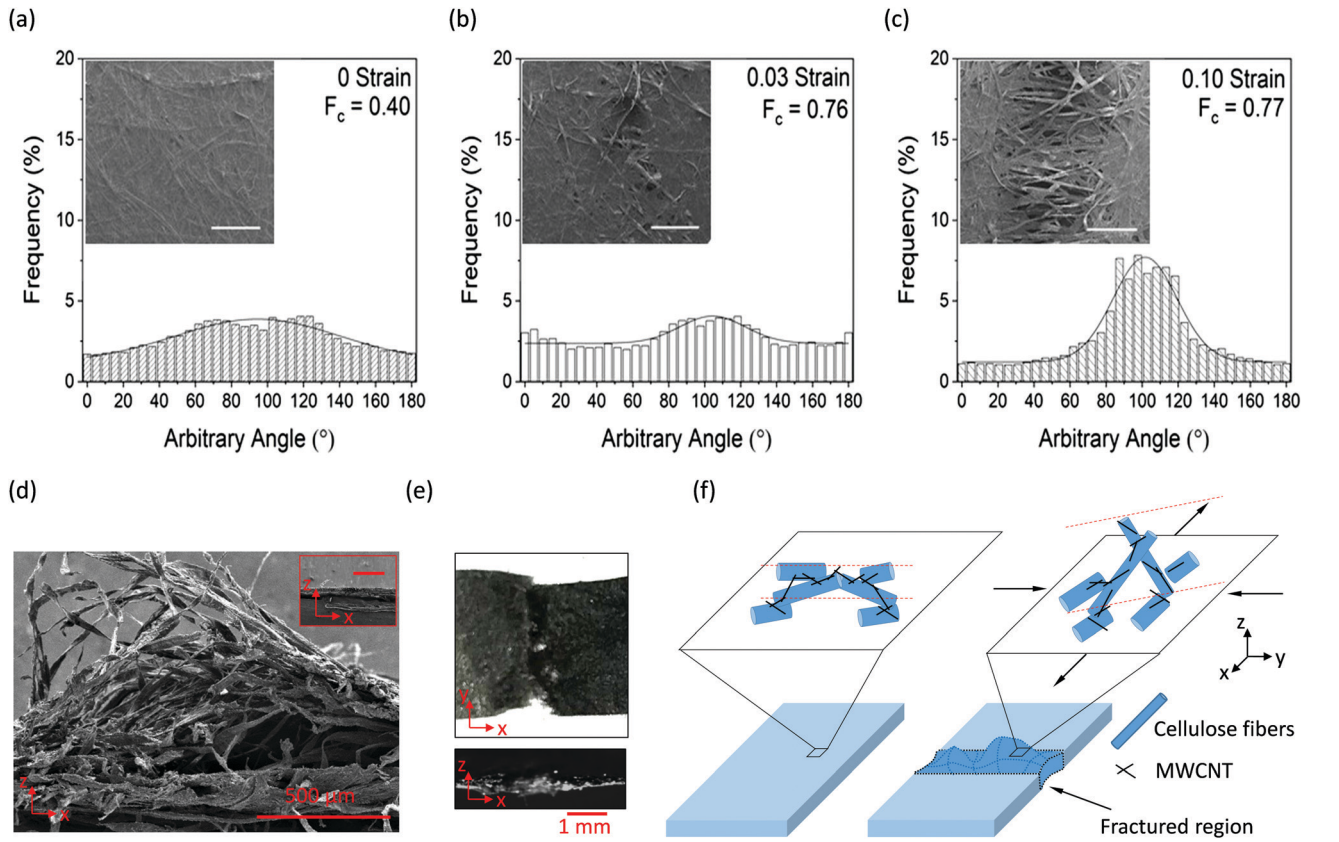

Fig. 3 (a–c) SEM images and fiber orientation of 2.5 CNT wt%-CPC at strain of 0, 0.03, and 0.10. (Scale bar: 500 μm) (d) SEM image of fractured CPC with 10 CNT wt% at strain of 0.10. Inset: SEM image of pristine CPC. (e) Schematic of fracture-induced x–z planar structure reorganization under stretching.

largest, as observed in the out-of-plane view. The smallest width of the fracture region was 3.8 mm, which was reduced by 23% compared to the original width.

The remarkable auxetic behavior of water-printed CPC resulted from the buckled fibers in the cellulose network under localized fracture. Upon fracture initiation, some inter-fiber junctions were weakened by water-printing and thus more readily disrupted. The breakage of the hydrogen bonds between cellulose fibers allowed for higher mobility of randomly distributed fibers, as demonstrated by the increasing f_c with applied strain (Fig. 3a–c). As these random cellulose fibers were realigned in the stretching direction (x axis) by fracture, cellulose fibers at the necking region were compressed in the width direction (Fig. 3e), buckled, and forced each other into out-of-plane direction (Fig. 3f). Numerous buckled cellulose fibers exhibited ridges and valleys along the x–y plane after fracture. As a result, the thickness was increased, resulting in a greater negative Poisson's ratio.

Our numerical and experimental results supported the auxetic mechanism (Fig. S8, ESI†). According to the stress concentration, the larger stress in x-direction was applied to the wet region, which resulted in the compression to the width direction (y-direction) with stretching. The compression-induced buckling expanded the CPC in z-direction. According to numerical simulation, in-plane necking and out-of-plane bulging were observed in Fig. S8d and g (ESI†). Experimentally, the bright and dark contrast of the cellulose fibers in the SEM images clearly shows the ridges and valleys in the inset of Fig. 3c and d. The spike of ν_{inst} at CPC's fracture strain also indicated that the auxeticity was induced by the buckling of cellulose fibers at fracture (Fig. 2a). Unlike the buckling of individual fibers in a previous report,[9] the fracture-induced buckling of cellulose fibers by water-printing exhibited the localized and predictable behaviors of fibers' due to the selectively reduced strength of inter-fiber junctions and the stress concentrations.

According to the orientation factors and Poisson's ratios of CPC with different CNT contents, the higher CNT contents led to reduce in-plane realignment of cellulose fibers, as well as decrease auxeticity. As a decisive factor of the auxetic behavior, the buckling of the cellulose fibers required the strong contacts between cellulose fibers to resist the inter-fiber slippage. As water-weakened hydrogen bonds between cellulose fibers were broken under stretching, intact hydrogen bonds served as contact points that pinned adjacent cellulose fibers supporting fiber reorientation and the formation of fiber ridges and valleys upon buckling. However, the presence of CNTs inhibited inter-fiber interactions, and resulted in sliding of cellulose fibers under stretching, rather than buckling. The sliding of cellulose fibers prohibited their orientation changes, thereby resulting in the lower degree of reorientation and thus, the lower auxeticity of CPC. This conclusion agreed with the larger auxeticity of CPC with the lower CNT contents (Fig. 2d).

The Poisson's ratio describing the auxetic behavior was described with a global strain not a local strain as shown in eqn (1) and (2). It was appropriate to use a global strain rather than a local strain because the stress concentration due to different Young's moduli and Poisson's ratios was the main factor for the large auxeticity. The large property difference of the wet and dry regions caused the stress concentration to increase the auxetic behavior. The stress concentration resulted in the necking of the wet region, and the subsequent larger buckling of the cellulose fibers. Hence, the Poisson's ratio was computed by the global strain not by the local strain.

Sensing performance and applications of CPC piezoresistive sensor

The CPC piezoresistive sensor showed high sensitivity with large dynamic range. The piezoresistive response was characterized for the pressure range of 0–500 kPa (Fig. 4a). The sensitivity showed a descending trend as the applied pressure increased. The empirical correlation between the normalized resistance of 10 wt%-CPC and the applied pressure (P) was:

$$\Delta R_{norm} = 9.0 \times 10^{-16}p^6 - 1.0 \times 10^{-12}p^5 + 1.0 \times 10^{-9}p^4 - 3.0 \times 10^{-7}p^3 + 5.0 \times 10^{-5}p^2 - 0.0038\,p + 0.99 \quad (4)$$

where ΔR_{norm} is the normalized resistance of 10 wt%-CPC. The linearized sensitivities of 2.5, 5, and 10 wt%-CPC are shown in the pressure range of 0–50 kPa (Fig. 4b). In addition to the fracture induced by straight line water-printing, a V-shaped fracture could also be generated by water-printing. The sensitivity of V-shaped CPC with 10 wt% was compared to assess the effect of fracture area on sensitivity. As shown by the inset of Fig. 4b, the V-shaped CPC showed greater fracture area compared to the straightly fractured CPC. The sensitivities of 2.5, 5, 10 wt%-CPC, and V-shaped 10 wt%-CPC were $(9.0 \pm 5.0) \times 10^{-3}$, $(4.1 \pm 1.4) \times 10^{-3}$, $(2.4 \pm 0.12) \times 10^{-3}$, and $(3.3 \pm 0.25) \times 10^{-3}$ kPa^{-1}, respectively. The sensitivity of "V" shape-fractured sensors showed 1.38 times that of the straightly fractured sensors due to the 40% larger fracture area. The increase of the fracture area led to the sensitivity increase by the similar ratio, which proposed the facile methodology of manipulating the sensitivity of the piezoresistive sensor by producing a water-printed fracture pattern.

The repeatability of a CPC piezoresistive sensor was measured for 10 000 cycles at different compressive pressure (Fig. 4c). For the cyclic pressure of 0–40 kPa, the sensor showed consistent resistance change. The sensing repeatability under smaller compressive loads was also demonstrated using a silicone block to apply a cyclic pressure of 50 Pa, which was successfully detected by the normalized resistance change of 0.02 (Fig. 4d).

The CPC piezoresistive sensor exhibited an extremely low detection limit. Fig. 4e shows the detection of very small pressures <10 Pa. The water drops of 10 and 100 μL were applied on a thin film placed above the fracture area of the sensor, with the contact area of 16 and 78 mm^2, respectively. The 10 μL water drop applied a pressure of only 6 Pa, resulting in a sensitivity of 3.3 kPa^{-1}. Opportunities exist to improve the detection limit further by designing CPC with greater fractured area. Note that the sensitivity could vary depending on the contact condition between an object and the sensor surface.

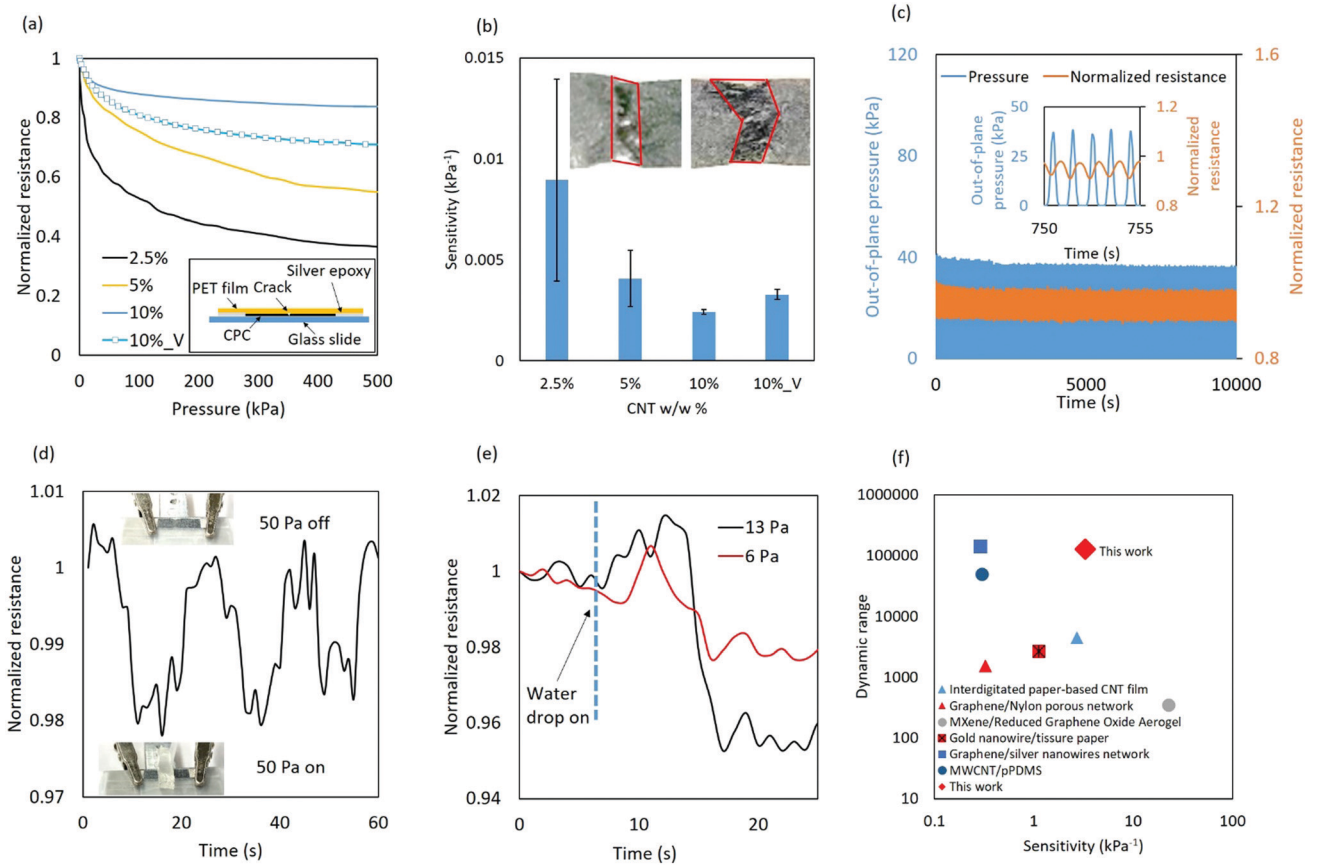

Fig. 4 Characterization of sensing performance of CPC piezoresistive sensor. (a) Normalized resistance response of CPC sensors with CNT wt % of 2.5, 5, 10, and 10 with V-shaped pattern under applied pressure from 0–500 kPa. Inset: Packaging of the pressure sensor. (b) Average sensitivity of CPC sensors with CNT wt% of 2.5, 5, 10, and 10 with V-shaped pattern under applied pressure from 0–50 kPa. Inset: Fractured shape induced by straight line and V-shaped water-printing. (c) Normalized resistance response of CNT-cellulose piezoresistive pressure sensor (thickness: 100 μm) to cyclic loads of 0–40 kPa. Inset: Closeup of normalized resistance response for 750–755 s. The CPC sensor is sealed with a polyethylene terephthalate (PET) film to avoid damaging the sensing element. (d) Cyclic detection of small pressure of 50 Pa. Inset: Images of sensor surface with and without the weight block. (e) Resistance changes of the CPC sensor when detecting a small drop of water with applied pressure of 6 Pa and 13 Pa, respectively. (f) Comparison of piezoresistive sensors for their sensitivity and dynamic range.[43–48]

For example, the water contact on the sensor surface was more uniform than the silicone block, which resulted in the higher sensitivity.

The high sensitivity of a CPC piezoresistive sensor was attributed to the dramatic disconnections and reconnections of the molecular junctions in conjunction with the extreme auxeticity. Numerous electrical paths were established on as-prepared CPC, as demonstrated by the SEM that shows evenly dispersed CNTs on random network of cellulose fibers (Fig. S1, ESI†). The electrical paths broken by the fracture could be reconnected under the applied pressure, resulting in piezosensitivity. As the distance between CNTs became greater than the tunneling distance, the resistance increased according to the power law.[24] The out-of-plane directional pressure reduced the distance between CNTs and induced the intensive recovery of the CNT connections. Hence, the piezoresistive sensors fabricated from the locally auxetic CPC demonstrated excellent sensitivity. In comparison to other random-network sensors, our sensors showed the outstanding performance in the sensitivity and dynamic range (Fig. 4f).

Using the fabricated sensors, various wearable applications could be conceived at low cost. A heartbeat sensor capable of measuring the rate of cardiovascular pulsations when wrapped around the wrist of an individual was fabricated (Fig. 5a). The cyclic motion from thoracic or abdominal expansions and contractions during inhalation and exhalation was also detected by mounting a CPC piezoresistive sensor on a belt, as depicted in Fig. 5b. The belt tension was adjusted such that the respiration motion could generate adequate relative pressure. The pressure difference between a human body and a sensor could be captured by a CPC sensor. The sensor is insensitive to the belt strain because of the sensor covered with a PET film. This offered an inexpensive and reliable way of monitoring breathing patterns for applications in sports and neonatal care.[49–51] In addition, a CPC sensor attached to an insole was able to monitor the gait movement based on foot pressure. Step count could be extracted from the piezoresistive signal. Walking, running, and jumping motions were clearly discriminated in the waveforms (Fig. 5c). The gait monitoring tests further confirmed that CPC sensors could

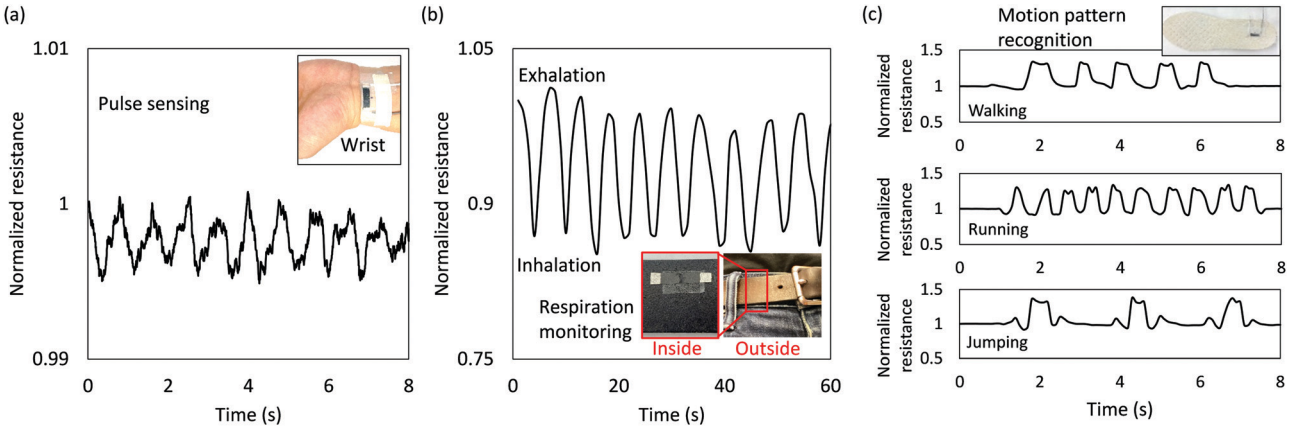

Fig. 5 Wearable sensor applications with CPC piezoresistive sensors. (a) Resistance variance of CPC pulse sensor when detecting wearer's pulse. Inset: Images of the CPC pulse sensor attached to the wearer's wrist. (b) Normalized resistance of the smart belt during normal respiration. (c) Resistance changes of a foot pressure sensor at three modes of motions: walking, running, and jumping. The CPC sensor is sealed with a polyethylene terephthalate (PET) film to avoid damaging the sensing element.

sustain repeated stress at elevated pressure without hindering the sensing performance.

Conclusion

In summary, the controlled auxeticity of a random fibrous network comprising a cellulose paper composite grafted with carbon nanotubes was investigated in combination with an innovative water-printing method. The CPC was locally fractured with necking along a water-printed region due to the reduced CPC strength and stress concentrations. Due to the wetting–stretching method, the fracture process of CPC was reproducibly manipulated with six-time water-printing. It was discovered that the amplified auxetic behavior was a result of the buckling of wet CPC matrix during fracture. The effective Poisson's ratio of water-printed CPC achieved a value of −49.5. The auxetic behavior of CPC improved the piezoresistive sensitivity through the recovery of terminated electrical pathways upon applied pressure. A remarkable piezoresistive sensitivity of 3.3 kPa^{-1} and a wide sensing range of 6–500 000 Pa were achieved. Tailoring auxeticity of a random matrix paper-based composite offers a new route to enhancing the piezoresistive sensitivity with the improved manufacturing reproducibility toward wearable applications, for instance, the gait and respiration detection.

Conflicts of interest

There are no conflicts of interest to declare.

Acknowledgements

SMG, HGW, ABD, and JHC acknowledge the support from the Advanced Manufacturing Program of National Science Foundation (No. 1927623). JZ and JC acknowledge the partial support of the CoMotion Innovation Fund at University of Washington. JC acknowledges partial support from IP group fund. The authors thank Zhongjie Qian for his help with the cyclic loading experiments.

References

1 R. Peng, Y. Ma, Q. Wu, B. Huang and Y. Dai, *Nanoscale*, 2019, **11**, 11413–11428.
2 D. Y. Fozdar, P. Soman, J. W. Lee, L. H. Han and S. Chen, *Adv. Funct. Mater.*, 2011, **21**, 2712–2720.
3 K. E. Evans and A. Alderson, *Adv. Mater.*, 2000, **12**, 617–628.
4 O. Duncan, T. Shepherd, C. Moroney, L. Foster, P. D. Venkatraman, K. Winwood, T. Allen and A. Alderson, *Appl. Sci.*, 2018, **8**, 941.
5 R. Lakes, *Science*, 1987, **238**, 551.
6 J. Dirrenberger, S. Forest, D. Jeulin and C. Colin, *Proc. Eng.*, 2011, **10**, 1847.
7 C. Borcea and I. Streinu, *Proc. R. Soc. A*, 2015, **471**, 20150033.
8 C. Körner and Y. Liebold-Ribeiro, *Smart Mater. Struct.*, 2014, **24**, 025013.
9 S. Domaschke, A. Morel, G. Fortunato and A. E. Ehret, *Nat. Commun.*, 2019, **10**, 1–8.
10 G. Schwartz, B. C.-K. Tee, J. Mei, A. L. Appleton, D. H. Kim, H. Wang and Z. Bao, *Nat. Commun.*, 2013, **4**, 1–8.
11 M. Kaltenbrunner, T. Sekitani, J. Reeder, T. Yokota, K. Kuribara, T. Tokuhara, M. Drack, R. Schwödiauer, I. Graz and S. Bauer-Gogonea, *Nature*, 2013, **499**, 458–463.
12 Y. Yamamoto, S. Harada, D. Yamamoto, W. Honda, T. Arie, S. Akita and K. Takei, *Sci. Adv.*, 2016, **2**, e1601473.
13 S. Zheng, X. Wu, Y. Huang, Z. Xu, W. Yang, Z. Liu, S. Huang, B. Xie and M. Yang, *Composites, Part A*, 2019, **121**, 510–516.
14 P. Wu, A. Xiao, Y. Zhao, F. Chen, M. Ke, Q. Zhang, J. Zhang, X. Shi, X. He and Y. Chen, *Nanoscale*, 2019, **11**, 21103–21118.
15 Y. Ding, J. Yang, C. R. Tolle and Z. Zhu, *ACS Appl. Mater. Interfaces*, 2018, **10**, 16077–16086.
16 Z. Zhou, Y. Li, J. Cheng, S. Chen, R. Hu, X. Yan, X. Liao, C. Xu, J. Yu and L. Li, *J. Mater. Chem. C*, 2018, **6**, 13120–13127.

17 Y. Wu, I. Karakurt, L. Beker, Y. Kubota, R. Xu, K. Y. Ho, S. Zhao, J. Zhong, M. Zhang and X. Wang, *Sens. Actuators, A*, 2018, **279**, 46–52.
18 S. Lim, D. Son, J. Kim, Y. B. Lee, J. K. Song, S. Choi, D. J. Lee, J. H. Kim, M. Lee and T. Hyeon, *Adv. Funct. Mater.*, 2015, **25**, 375–383.
19 M. Amjadi, K. U. Kyung, I. Park and M. Sitti, *Adv. Funct. Mater.*, 2016, **26**, 1678–1698.
20 M. Amjadi, A. Pichitpajongkit, S. Lee, S. Ryu and I. Park, *ACS Nano*, 2014, **8**, 5154–5163.
21 J. J. Park, W. J. Hyun, S. C. Mun, Y. T. Park and O. O. Park, *ACS Appl. Mater. Interfaces*, 2015, **7**, 6317–6324.
22 M. Hempel, D. Nezich, J. Kong and M. Hofmann, *Nano Lett.*, 2012, **12**, 5714–5718.
23 C. S. Boland, U. Khan, C. Backes, A. O'Neill, J. McCauley, S. Duane, R. Shanker, Y. Liu, I. Jurewicz and A. B. Dalton, *ACS Nano*, 2014, **8**, 8819–8830.
24 J. Zhang, G. Y. Lee, C. Cerwyn, J. Yang, F. Fondjo, J. H. Kim, M. Taya, D. Gao and J. H. Chung, *Adv. Mater. Technol.*, 2018, **3**, 1700266.
25 J. Ko, S. Bhullar, Y. Cho, P. C. Lee and M. B.-G. Jun, *Smart Mater. Struct.*, 2015, **24**, 075027.
26 M. F. Ahmed, Y. Li and C. Zeng, *Mater. Chem. Phys.*, 2019, **229**, 167–173.
27 Y. Jiang, Z. Liu, N. Matsuhisa, D. Qi, W. R. Leow, H. Yang, J. Yu, G. Chen, Y. Liu and C. Wan, *Adv. Mater.*, 2018, **30**, 1706589.
28 C.-J. Lee, K. H. Park, C. J. Han, M. S. Oh, B. You, Y.-S. Kim and J.-W. Kim, *Sci. Rep.*, 2017, **7**, 1–8.
29 S. P. Lacour, D. Chan, S. Wagner, T. Li and Z. Suo, *Appl. Phys. Lett.*, 2006, **88**, 204103.
30 Y. Li, S. Luo, M. C. Yang, R. Liang and C. Zeng, *Adv. Funct. Mater.*, 2016, **26**, 2900–2908.
31 P. Verma, M. L. Shofner and A. C. Griffin, *Phys. Status Solidi B*, 2014, **251**, 289–296.
32 N. Stenberg and C. Fellers, *Nord. Pulp Pap. Res. J.*, 2002, **17**, 387–394.
33 H. Liu, H. Jiang, F. Du, D. Zhang, Z. Li and H. Zhou, *ACS Sustainable Chem. Eng.*, 2017, **5**, 10538–10543.
34 Y. Wei, S. Chen, F. Li, Y. Lin, Y. Zhang and L. Liu, *ACS Appl. Mater. Interfaces*, 2015, **7**, 14182–14191.
35 C. Yan, J. Wang, W. Kang, M. Cui, X. Wang, C. Y. Foo, K. J. Chee and P. S. Lee, *Adv. Mater.*, 2014, **26**, 2022–2027.
36 C. Casiraghi, M. Macucci, K. Parvez, R. Worsley, Y. Shin, F. Bronte, C. Borri, M. Paggi and G. Fiori, *Carbon*, 2018, **129**, 462–467.
37 A. Dichiara, A. Song, S. Goodman, D. He and J. Bai, *J. Mater. Chem. A*, 2017, **5**, 20161–20169.
38 S. M. Goodman, N. Ferguson and A. B. Dichiara, *RSC Adv.*, 2017, **7**, 5488–5496.
39 S.-J. Kahng, C. Cerwyn, B. M. Dincau, J.-H. Kim, I. V. Novosselov, M. Anantram and J.-H. Chung, *Nanotechnology*, 2018, **29**, 335304.
40 P. Verma, M. L. Shofner, A. Lin, K. B. Wagner and A. C. Griffin, *Phys. Status Solidi B*, 2015, **252**, 1455–1464.
41 G. T. Pham, Y.-B. Park, Z. Liang, C. Zhang and B. Wang, *Composites, Part B*, 2008, **39**, 209–216.
42 H. Qi, B. R. Schulz, T. Vad, J. Liu, E. Mäder, G. Seide and T. Gries, *ACS Appl. Mater. Interfaces*, 2015, **7**, 22404–22412.
43 C. Wang, X. Hou, M. Cui, J. Yu, X. Fan, J. Qian, J. He, W. Geng, J. Mu and X. Chou, *Sci. China Mater.*, 2020, **63**, 403–412.
44 Z. He, W. Chen, B. Liang, C. Liu, L. Yang, D. Lu, Z. Mo, H. Zhu, Z. Tang and X. Gui, *ACS Appl. Mater. Interfaces*, 2018, **10**, 12816–12823.
45 Y. Ma, Y. Yue, H. Zhang, F. Cheng, W. Zhao, J. Rao, S. Luo, J. Wang, X. Jiang and Z. Liu, *ACS Nano*, 2018, **12**, 3209–3216.
46 S. Gong, W. Schwalb, Y. Wang, Y. Chen, Y. Tang, J. Si, B. Shirinzadeh and W. Cheng, *Nat. Commun.*, 2014, **5**, 1–8.
47 X. Dong, Y. Wei, S. Chen, Y. Lin, L. Liu and J. Li, *Compos. Sci. Technol.*, 2018, **155**, 108–116.
48 R. Iglio, S. Mariani, V. Robbiano, L. Strambini and G. Barillaro, *ACS Appl. Mater. Interfaces*, 2018, **10**, 13877–13885.
49 S. D. Min, Y. Yun and H. Shin, *IEEE Sens. J.*, 2014, **14**, 3245–3251.
50 X. A. Li, C. Stepaniak and E. Gore, *Med. Phys.*, 2006, **33**, 145–154.
51 S. W. Park, P. S. Das, A. Chhetry and J. Y. Park, *IEEE Sens. J.*, 2017, **17**, 6558–6564.